

The coalescing colony model: mean-field, scaling, and geometry

Giulia Carra, Kirone Mallick, Marc Barthelemy

▶ **To cite this version:**

Giulia Carra, Kirone Mallick, Marc Barthelemy. The coalescing colony model: mean-field, scaling, and geometry. Physical Review E : Statistical, Nonlinear, and Soft Matter Physics, 2017, 96, pp.062316. 10.1103/PhysRevE.96.062316 . cea-01626261

HAL Id: cea-01626261

https://cea.hal.science/cea-01626261

Submitted on 30 Oct 2017

HAL is a multi-disciplinary open access archive for the deposit and dissemination of scientific research documents, whether they are published or not. The documents may come from teaching and research institutions in France or abroad, or from public or private research centers.

L'archive ouverte pluridisciplinaire **HAL**, est destinée au dépôt et à la diffusion de documents scientifiques de niveau recherche, publiés ou non, émanant des établissements d'enseignement et de recherche français ou étrangers, des laboratoires publics ou privés.

arXiv:1709.08628v1 [q-bio.PE] 25 Sep 2017

The coalescing colony model: mean-field, scaling, and geometry

Giulia Carra and Kirone Mallick
Institut de Physique Théorique, CEA, CNRS-URA 2306, F-91191, Gif-sur-Yvette, France

Marc Barthelemy*
Institut de Physique Théorique, CEA, CNRS-URA 2306, F-91191, Gif-sur-Yvette, France and Centre d'Analyse et de Mathématique Sociales, (CNRS/EHESS) 190-198, avenue de France, 75244 Paris Cedex 13, France

We analyze the coalescing model where a 'primary' colony grows and randomly emits secondary colonies that spread and eventually coalesce with it. This model describes population proliferation in theoretical ecology, tumor growth and is also of great interest for modeling the development of cities. Assuming the primary colony to be always spherical of radius $r(t)$ and the emission rate proportional to $r(t)^\theta$ where $\theta > 0$, we derive the mean-field equations governing the dynamics of the primary colony, calculate the scaling exponents versus θ and compare our results with numerical simulations. We then critically test the validity of the circular approximation and show that it is sound for a constant emission rate ($\theta = 0$). However, when the emission rate is proportional to the perimeter, the circular approximation breaks down and the roughness of the primary colony can not be discarded, thus modifying the scaling exponents.

Keywords: Statistical Physics — Dispersal problem — Complex systems modeling

Dispersal models have been used extensively to investigate the proliferation of animal colonies in theoretical ecology [1, 2] and as a simplified model for the growth of cancerous tumors [3, 4]. Such models are also good candidates for describing the growth of the built-area of cities [5] for which we now have empirical data over long periods of time [6]. The main feature of dispersal models is the concomitant existence of two growth mechanisms. The first process is the growth of the main – so-called primary – colony, which occurs via a reaction-diffusion process (as described by a FKK-like equation [7, 8]) and leads to a constant growth with velocity c, depending on the details of the system. The second ingredient is *random dispersal* from the primary colony, which represents the emergence of secondary settlements in the framework of animal ecology, the development of metastatic tumors, or, in the urban sprawl case, the creation of small towns in the periphery of large cities. In the real world, dispersion follows privileged directions under the effect of external forces such as blood vessels, winds and rivers, or transportation networks for cities but in a first approach, these anisotropic effects will be neglected. We will assume that secondary colonies also grow at the velocity c and will eventually coalesce with the primary colony, leading to a larger primary colony whose time-dependent size will depend on the emission rate.

A classical way to study dispersal is through the *dispersal kernel* representing the probability distribution of dispersal distances and various forms for these kernels have been discussed [9]. A different approach has been introduced by Kawasaki and Shigesada in [1, 8] who proposed the use of simple models to tackle this challenging problem. We shall follow this point of view and study the *coalescing colony model* where a primary colony grows at radial velocity c and emits a secondary colony at a rate λ and at a distance ℓ from its border (long-range dispersal). The variable ℓ can be drawn from a probability distribution $P(\ell)$ but we consider here that the secondary colonies are emitted at a constant distance ℓ_0 from the boundary of the primary colony (i.e. $P(\ell) = \delta(\ell - \ell_0)$). Besides, we assume that each secondary colony also grows with the same radial speed c and does not emit tertiary colonies. The dependence of the emission rate on the colony size is taken into account by the functional form

$$\lambda(r) = \lambda_0 r^\theta \ , \tag{1}$$

r being the radius of the primary colony and $\theta \geq 0$. When $\theta = 0$ the growth rate is independent from the primary colony size, for $\theta = 1$ it is proportional to its perimeter and for $\theta = 2$ to its area.

Coalescence happens when a secondary colony of radius r_2 intersects with the primary one, of radius r, and becomes part of the latter. We shall consider two variants of the process. In the first version of the model, denoted by the M_0 model, we assume that the primary colony remains circular after coalescence (see Fig. 1), and has a new radius r' given by

$$r'^2 = r^2 + r_2^2 \ . \tag{2}$$

This interesting model was discussed in [8] but a full quantitative understanding of the radius $r(t)$ is still lacking. Here, we present a microscopic derivation of the dynamics of the M_0 model, in the mean-field approximation, and study its solutions as a function of the parameter θ. In particular, we derive a simplified equation that preserves the physics of the system and allows to extract the scaling behavior for the main quantities of interest. Our predictions are then tested with numerical simulations.

In the second part of this work, we discuss the importance of the circular approximation and its impact on the scaling behaviors. We introduce a modified version of the process, referred to as the M_1 model, in which after coalescence the secondary colony merges into the primary colony and the shape of the primary colony does not remain circular. This important difference between models M_0 and M_1 is illustrated in the Fig. 1.

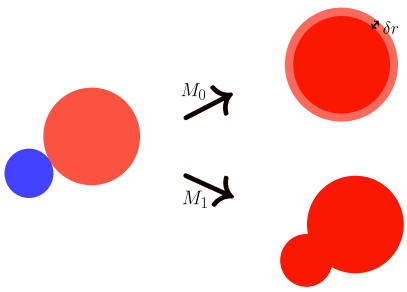


FIG. 1: Example of coalescence in models M_0 and M_1. In M_0, the primary colony (in red) remains circular and the area of the secondary colony is evenly distributed on the rim; in M_1, the shapes are simply 'concatenated'.

We now derive the main equations for the model M_0. We recall that $\lambda(t_i)dt_i$ represents the probability to emit a colony in the interval $[t_i, t_i + dt_i]$ and we denote by $t_i{}'$ the time of coalescence of a colony emitted at time t_i. The condition of coalescence is given by

$$r(t_i{}') + ct_i{}' = \ell_0 + r(t_i) + ct_i \ , \tag{3}$$

which defines – formally – the function f such that

$$t_i{}' = f(t_i) \ . \tag{4}$$

The mean-field approach that we propose here consists in neglecting the fluctuations of this function $f(t)$ and to consider that it is the same for all secondary colonies. The evolution of the area of the primary colony is thus given by

$$\frac{dA}{dt} = 2\pi rc + \int dt_i \lambda(t_i)\delta(t - f(t_i))\pi c^2 (t - t_i)^2 \ , \tag{5}$$

where the first term of the rhs is due to short-range dispersion and the second term represents the coalescence with secondary colonies. This leads to

$$\frac{dA}{dt} = 2\pi rc + \lambda(f^{-1}(t)) \mid \left[f^{-1}(t)\right]' \pi c^2 (t - f^{-1}(t))^2 \mid \ . \tag{6}$$

We call $x(t)$ the radius of the colony absorbed at time t, given by $x(t) = c(t - f^{-1}(t))$. Injecting this quantity in Eqs. (3) and (6), we obtain the Kawasaki-Shigesada system of equations [8]

$$\begin{cases} \dfrac{dr}{dt} = c + \dfrac{\lambda_0 \left[r\left(t - \frac{x(t)}{c}\right)\right]^\theta}{2\pi r(t)} \left(1 - \dfrac{\dot{x}(t)}{c}\right) \pi x(t)^2 \ , & (7) \\ \ell_0 = r(t) - r\left(t - \dfrac{x(t)}{c}\right) + x(t) \ . & (8) \end{cases}$$

In the long time regime, $t \gg x(t)/c$, the system of Eq. (7) and Eq. (8) takes the simplified form

$$\begin{cases} \dfrac{dr}{dt} = c + \dfrac{\lambda_0 r^{\theta-1}}{2} x(t)^2 \ , & (9) \\ x(t) = \dfrac{\ell_0}{1 + \frac{\dot{r}}{c}} \ . & (10) \end{cases}$$

These effective equations allow us to investigate the behavior of the model without altering the physics of the problem as will be shown by comparing the solutions to numerical simulations.

We first solve the effective system for $\theta = 0$ (ie. $\lambda = \lambda_0$). Defining x^* as the average radius of a secondary colony just before its coalescence and assuming that it is constant in time we obtain

$$\frac{dr}{dt} = c + \frac{\lambda_0}{2r} x^{*2} \ , \tag{11}$$

whose solution is

$$r(t) \sim a + ct + \frac{\lambda_0 x^{*2}}{2c} \log\left(\frac{2cr}{\lambda_0 x^{*2}} + 1\right) \ . \tag{12}$$

When $t \to \infty$, the dominant contribution is

$$r(t) \sim a + ct + \frac{\mathscr{C}}{c} \log\left(\frac{c^2 t}{\mathscr{C}} + 1\right) \ , \tag{13}$$

with $x^* \simeq \ell_0/2$ and $\mathscr{C} = \frac{\lambda l_0^2}{8}$.

We perform numerical simulations with a constant $\lambda_0 = 0.5$ and $c = 1$, for different values of the emission distance ℓ_0. It is useful to introduce $\eta = \frac{2c}{l_0 \lambda_0}$, which represents the ratio between the emission time $\tau_e = 1/\lambda_0$ and the coalescence time $\tau_c = \ell_0/(2c)$. In Fig. 2 Top-Left, we plot the radius of the primary colony $r(t)$ versus t. We then perform on these data a two parameters fit with a function of the form

$$g(t) = a + \frac{\mathscr{C}_{simul}}{c} \log\left(\frac{c^2 t}{\mathscr{C}_{simul}} + 1\right) \ , \tag{14}$$

where the fitting parameters are a and $\mathscr{C}_{simul}$. In Fig. 2 Top-Right we test the results of the fit, comparing the estimated value $\mathscr{C}_{simul}$ obtained, with its theoretical value $\mathscr{C} = \frac{\lambda l_0^2}{8} = \frac{c^2}{2\lambda_0 \eta^2}$. We observe an excellent agreement, showing the validity of our theoretical calculations.

For $\theta > 1$, we further simplify the system Eqs. (26) and (27) by assuming $\dot{r} \gg c$ and obtain the single effective equation

$$Ar(t)^{\theta-1} \simeq \dot{r(t)}^2 \left(\dot{r(t)} - c\right) \tag{15}$$

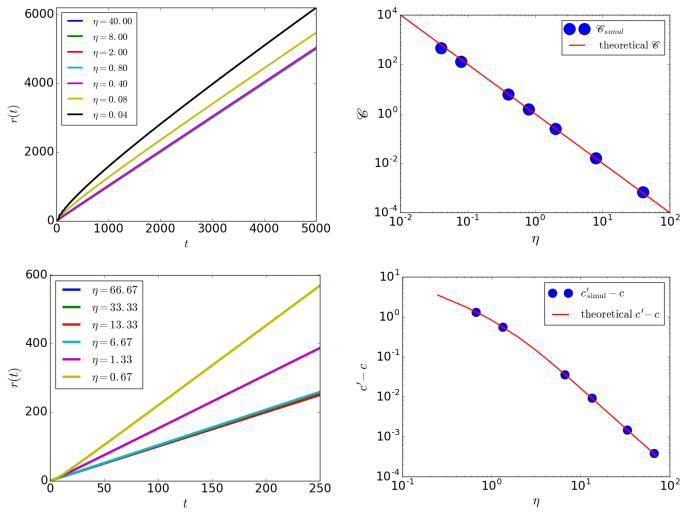


FIG. 2: (Top) Case $\theta = 0$: (Top-Left) Plot of $r(t)$ versus t for different values of the parameter η, averaged over 10 simulations. (Top-Right) Plot of $\mathscr{C}_{simul}$ versus η extracted from the empirical fit. The theoretical prediction is shown in red. (Bottom) Case $\theta = 1$: (Bottom-Left) $r(t)$ versus t for different values of the parameter η, obtained averaging over 100 simulations. (Bottom-Right) $c' - c$ versus η as obtained from the empirical fit. In red, the theoretical prediction (Eq. (18)).

with $A = \frac{\lambda_0}{2} c^2 \ell_0^2$. This nonlinear differential equation captures the physics of the coalescence and allows us to extract the large-time behavior of the main quantities of interest in this problem. In particular, assuming scaling laws at large times of the form $r(t) \sim a t^\beta$ and $x(t) \sim d t^{-\alpha}$, Eq. 15 yields

$$\beta = \frac{3}{4-\theta} , \qquad \alpha = \beta - 1 . \tag{16}$$

Note that for $\theta \to 4$, we have $\beta \to \infty$, the radius grows faster than a power law and explodes exponentially. For $\theta = 1$, we obtain $\alpha = 0, \beta = 1$ which means that we have $x(t) = x^*$ independent of t and a linear behavior of $r(t)$. From Eq. (7) we deduce that the radial velocity c' is given by

$$c' = c + \frac{\lambda_0}{2} x^{*2} \tag{17}$$

and the value of x^* can be obtained by solving Eq. (8) that can be written as

$$\frac{\lambda_0}{2c} x^{*3} + 2x^* - \ell_0 = 0 . \tag{18}$$

This result, for the specific case of $\theta = 1$, was first obtained by Shigesada and Kawasaki [1]. We test this result numerically (with $\lambda_0 = 0.3$, $c = 1$, and for different values of the emission distance ℓ_0) and in Fig. 2 Bottom-Left we plot the radius of the primary colony $r(t)$ versus t. A linear fit allows us to obtain an estimate for the radial velocity c' that we compare in Fig. 2 Bottom-Right with the theoretical prediction of Eq. (18). Here also, an excellent agreement is observed.

For $\theta > 1$, the theoretical analysis predicts that the leading order characterized by a scaling behavior given by Eqs. (16) can be observed in a range of time $t_{min} \ll t \ll t_{max}$ which depend on θ and on the parameter $\eta^2\lambda/2$ (see the supplementary material for details on this point). We performed numerical simulations for $\theta = [1.1, 1.2, 1.3, 1.4, 1.6, 2.0]$, with the parameter $c = 1$ and $\lambda = 0.001$ (and additional simulations with the parameter $\lambda = 0.005$ for $\theta = 1.2$). In Fig. 3, we plot the values of the exponents β obtained by power law fits and we compare it with the theoretical prediction (Eq. (16)) in red. We observe a good agreement with some deviations for higher values of θ which is probably due the small range $[t_{min}, t_{max}]$ in this case.

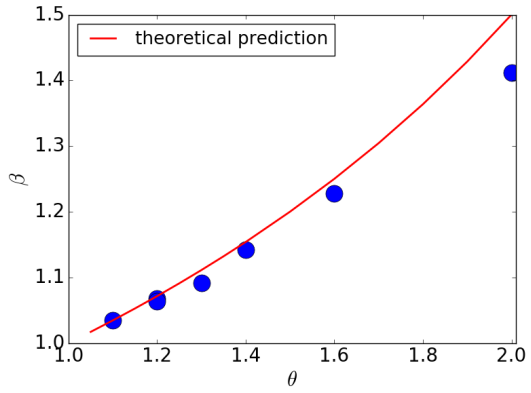


FIG. 3: Plot of the exponent β as a function of θ, obtained from a power law fit on $r(t)$ versus t for the values of $\eta^2\lambda/2$ maximizing the range $[t_{min}, t_{max}]$ in our simulation domain.

The Shigesada-Kawasaki coalescing model is based on the circular approximation. The validity of this hypothesis will be investigated by simulating the M_1 model where we respect the geometry of the coalescence process. We first consider a constant emission rate $\lambda(r) = \lambda_0$ and assume that the area A and the perimeter P obey to a power law scaling of the form

$$A(t) \sim t^\mu \qquad P(t) \sim t^\nu . \tag{19}$$

Performing a power-law fit on the empirical results, we obtain $\mu \approx 2$ and $\nu \approx 1$ (see Supplementary Material for details and plots). These results can be compared with those obtained in the model M_0. In Fig. 4, we plot $A(t)/(\pi c^2 t^2) - 1$ and $P(t)/(2\pi c t) - 1$ versus t: these

quantities both go to zero for large values of t, suggesting that at large times, the dominant behavior of the M_0 and the M_1 models are the same with $A(t) \sim \pi c^2 t^2$ and $P(t) \sim 2\pi ct$. Hence, for $\theta = 0$ and large value of t, the circular approximation appears to be valid. If we assume

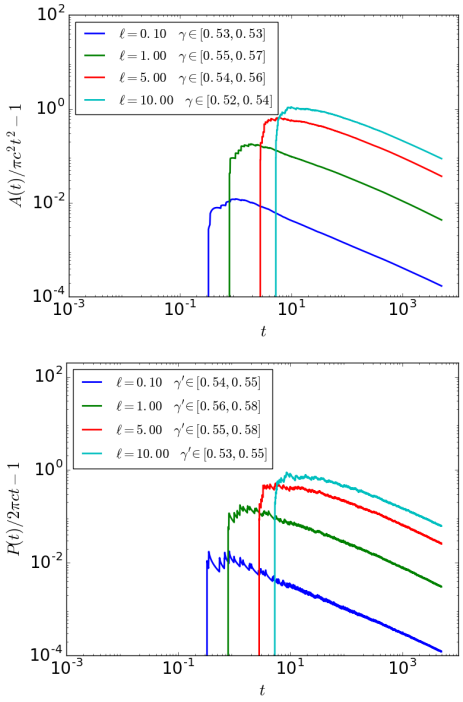


FIG. 4: (Left) $A(t)/(\pi c^2 t^2) - 1$ versus time t. (Right) $P(t)/(2\pi ct) - 1$ versus t. These results are obtained for different values of ℓ and are averaged over 100 numerical simulations. For each value of ℓ, we report in the inset the values of the exponents γ and γ' obtained by fitting these plots.

that the sub-dominant corrections are described by the scaling forms

$$\frac{A(t)}{\pi c^2 t^2} - 1 \sim t^{-\gamma} \qquad \frac{P(t)}{2\pi ct} - 1 \sim t^{-\gamma'} \tag{20}$$

the numerical results suggest that $\gamma \sim 0.5$ and $\gamma' \sim 0.5$ showing that the corrections to the dominant term are decaying as a power law in model M_1, in contrast with the logarithmic correction observed in the M_0 model (see Supplementary Material).

We now focus on the simulation results obtained for the M_1 model characterized by an emission rate λ given by

$$\lambda(t) = \lambda_0 P(t) \ , \tag{21}$$

where $P(t)$ is the total perimeter of the primary colony at time t, which corresponds to the case $\theta = 1$ in the model M_0. The simulations results for the area $A(t)$ and the perimeter $P(t)$ of the primary colony (see Supp. Mat.)

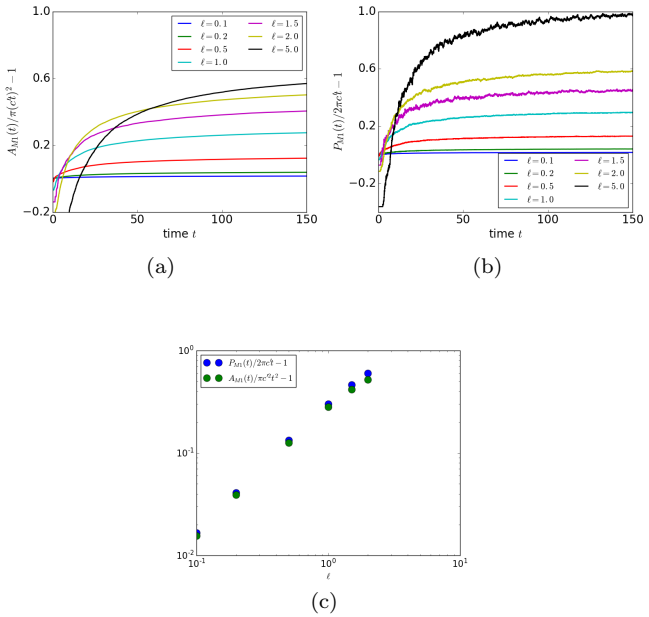


FIG. 5: (a) $A(t)/(\pi c^2 t^2) - 1$ versus t for different values of ℓ. (b) $P(t)/(2\pi ct) - 1$ versus t for different values of ℓ. (c) Plot of $f_1(\ell)$ and $f_2(\ell)$ versus ℓ for $t = 200$. These results are obtained by averaging over 100 simulations.

suggest that we still have $\mu \approx 2$ and $\nu \approx 1$ as in the M_0 model. We can go further and investigate the prefactor. We recall that for the M_0 model with $\theta = 1$, the radius of the primary colony increases with an effective radial velocity $c' > c$. In Fig. 5 we plot the quantities $A(t)/\pi c'^2 t^2 - 1$ and $P(t)/2\pi c' t - 1$; if the prefactor is the same of the M_0 model we should find (as we did for $\theta = 0$) that these quantities tend to zero for large values of t. In Fig. 5-(a)-(b), we see that these two quantities tend to a constant that depends on ℓ. We can therefore write

$$A(t) = \pi c'^2 (1 + f_1(\ell)) t^2 \qquad P(t) = 2\pi c' (1 + f_2(\ell)) t \ . \tag{22}$$

and we observe numerically that $f_1 \equiv f_2$ (see Fig. 5-(c)), demonstrating that the circular approximation is not appropriate for $\theta = 1$. In order to shed some light on this behavior, we plot the quantities $\frac{A(t)}{\pi \langle r \rangle^2} - 1$ and $\frac{P(t)}{2\pi \langle r \rangle} - 1$ where $\langle r \rangle$ is the average radius of the primary colony. The results shown in Fig. 6 suggest that the perimeter cannot be described by a circle, signaling a breakdown of the circular approximation (even if from the point of view of the area the system behaves approximately as a circle). To visualize the shape of the system, we consider a simplified picture where the primary colony is described as a circle of radius $\langle r \rangle$ to which n semicircles of average radius δ are attached (see Fig. 7 for an illustration). The maximum number of semicircles is $N = \frac{\pi \langle r \rangle}{\delta}$, and we

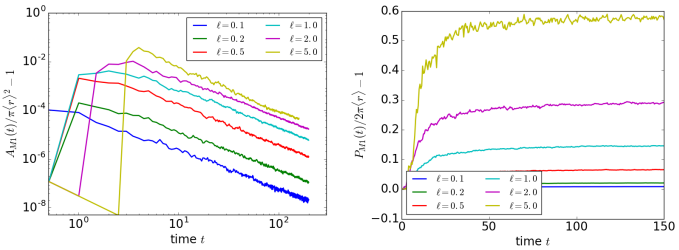


FIG. 6: (Left) $\frac{\pi\langle r\rangle^2}{A(t)} - 1$ versus t for different values of ℓ. (Right) $\frac{P(t)}{2\pi\langle r\rangle} - 1$ for different values of ℓ. The results are obtained averaging over 100 simulations.

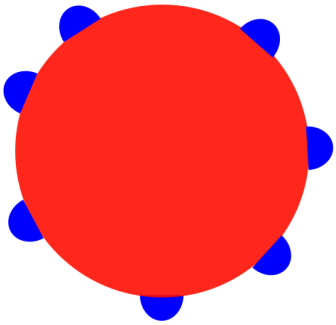


FIG. 7: A simplified representation of the primary colony in the model M_1 with $\theta = 1$ (here we have $n = 7$).

have for this toy model

$$\frac{P}{2\pi\langle r\rangle} - 1 = \frac{n}{N}\left(\frac{\pi}{2} - 1\right) \tag{23}$$

leading to a value in the range $[0, \frac{\pi}{2} - 1]$, consistent with the result of Fig. 6 (right). This figure also suggests that n increases with the dispersion distance ℓ, while for small value of ℓ the secondary colonies are quickly absorbed.

The circularity of the primary colony can be probed further with the observable

$$S(t) = P(t)/(2\sqrt{\pi A(t)}) - 1 \ . \tag{24}$$

For a perfect circle $S(t) = 0$, whereas $S(t) > 0$ estimates the 'rugosity' of the system. The results shown in Fig. 8(top) indicate that for $\theta = 0$, $S(t)$ is larger than zero but tends to zero for large values of t as expected from the previous discussion and the model M_0 seems to be a sound approximation when $\theta = 0$. But, for $\theta = 1$, this is not true anymore: we observe in Fig. 8(bottom) that $S(t) > 1$ and that $S(t)$ tends to a constant for large t, consistently with the previous results.

We developed the general framework allowing the theoretical discussion of the growth and coalescence process.

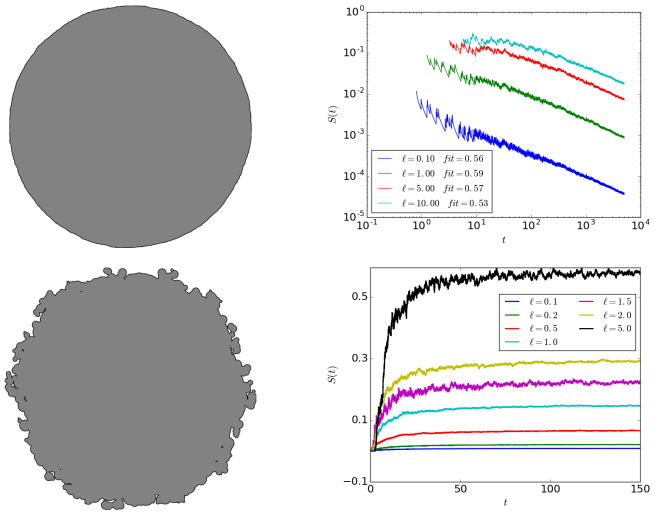


FIG. 8: (Left) Example of shapes obtained for the primary colony in the M_1 model. (Top-left) Case $\theta = 0$, $\ell = 10$. (Top-right) Case $\theta = 1$, $\ell = 2$. (right) $S(t)$ versus t. On the top we have the behavior for $\theta = 0$ averaged over 10 simulations and on the bottom $\theta = 1$ averaged over 100 simulations.

We discussed the quantitative predictions for the simpler model in which the emission rate depend on the exponent θ, while the distance ℓ is constant and the process is isotropic. However, it is possible to integrate other specific features such as anisotropy or random emission distances and to investigate how these latter modify the actual results. Also, the circular approximation that allows for this analytical approach seems to be justified in cases where the emission rate grows not too quickly with the size of the primary colony. Otherwise, it is necessary to take the geometry of the colony into account, and making the theoretical extremely challenging. This model is very general and versatile, the results obtained are potentially useful to gain insights into the understanding of population proliferation, tumor growth and is also of great interest for modeling the dynamics of complex systems such as the sprawl of cities.

Acknowledgments GC thanks the Complex Systems Institute in Paris (ISC-PIF) for hosting her during part of this work and for providing the OpenMole platform. MB thanks the city of Paris for its funding 'Paris 2030'.

* Electronic address: marc.barthelemy@ipht.fr

[1] N. Shigesada and K. Kawasaki, Invasion by stratified diffusion (Oxford University Press, USA, 1997), chap. 5, p. 79103.

[2] J. Clark, M. Lewis, and H. L., The American Naturalist, 157, 537 (2001).

[3] K. Iwata, K. Kawasaki, and N. Shigesada, J. theor. Biol. 203, 177 (2000).
[4] V. Haustein and U. Schumacher, J. Clin. Bioinforma. 2 (2012).
[5] M. Barthelemy, The Structure and Dynamics of Cities (Cambridge University Press, 2016).
[6] S. Angel, S. Sheppard, D. L. Civco, R. Buckley, A. Chabaeva, L. Gitlin, A. Kraley, J. Parent, and M. Perlin, The dynamics of global urban expansion (World Bank, Transport and Urban Development Department Washington, DC, 2005).
[7] R. A. Fisher, Annals of Human Genetics 7, 355 (1937).
[8] N. Shigesada and K. Kawasaki, Invasion and the range expansion of species: effects of long-distance dispersal (Blackwell Science, 2002), chap. 17, p. 350373.
[9] M. Lewis, S. Petrovskii, and J. Potts, The Mathematics Behind Biological Invasions (Springer International Publishing, 2016).

Supplementary material

The model M_0: further investigations

We discuss for $\theta > 1$ the range of validity of the power-law behavior $r(t) \sim t^\beta$, exploring the second order behavior.
Assuming the following form for the evolution of the radius of the primary colony with time,

$$r(t) \sim at^\beta + bt^{\beta'} \ , \tag{25}$$

we consider the simplified Shigesada-Kawasaki system of equations given by

$$\begin{cases} \dfrac{dr}{dt} = c + \dfrac{\lambda_0 r^{\theta-1}}{2} x(t)^2 \ , & (26) \\ x(t) = \dfrac{\ell_0}{1 + \frac{\dot{r}}{c}} \ ; & (27) \end{cases}$$

with $A = \frac{\lambda}{2} c^2 \ell_0^2$. After some calculations, a development at the first and second order of Eq. (26) bring to the following results

$$\beta' = 1 \ , \tag{28}$$

$$a = \left(\frac{2\beta^3}{\ell_0^2 \lambda_0 c^2} \right)^{\frac{1}{\theta-4}} \ , \tag{29}$$

and

$$b = \frac{4-\theta}{15-6\theta} \ . \tag{30}$$

Being all the parameters determined we can deduce the value of the time $t_{min} = (b/a)^{1/(\beta-1)}$ starting from which the second order term begins to be smaller than the first order one. Hence, for $t \gg t_{min}$ we can write $r(t) \sim at^\beta$, neglecting the second order term. After some calculation one gets

$$t_{min} = f(\theta) \left(\frac{2c^{2-\theta}}{\lambda_0 {\ell_0}^2} \right)^{\frac{1}{\theta-1}} \tag{31}$$

with

$$f(\theta) = \left(\frac{4-\theta}{15-6\theta} \right)^{\frac{4-\theta}{\theta-1}} \left(\frac{27}{(4-\theta)^3} \right)^{\frac{1}{\theta-1}} \ . \tag{32}$$

We remark moreover that the Shigesada-Kawasaki equations are valid only if the coalescence of a colony does not cause the coalescence of another secondary colony. This means that the increasing in the radius at time t, $\delta r(t)$ has to be smaller than the distance between two successively emitted secondary colonies. The following relation has to be verified

$$\sqrt{r^2 + {x^*}^2} - r < \frac{2c}{\lambda_0 r^\theta} \ . \tag{33}$$

From Eq. (27) one can write

$$x(t) \simeq \frac{c\ell_0}{\dot{r(t)}} \ , \tag{34}$$

this implies the following relation

$$x(t) \sim dt^{-\alpha} \tag{35}$$

with $\alpha = \beta - 1$ and $d = c\ell_0/(\beta a)$. After some calculations one can show that the Shigesada-Kawasaki system of equations is valid only for $t < t_{max}$, with

$$t_{max} = g(\theta) \left(\frac{2c^{2-\theta}}{\lambda_0 {\ell_0}^2} \right)^{\frac{1}{\theta-1}} \tag{36}$$

and

$$g(\theta) = 2^{\frac{4-\theta}{\theta-1}} \beta \ . \tag{37}$$

To summarize, we are able to observe the power-law behavior given by $r(t) \sim t^\beta$ in the range of time for which $t_{min} \ll t < t_{max}$. The size of the range of validity depends on the ratio between $g(\theta)$ and $f(\theta)$. This ratio decreases when θ increases as shown in Fig. 9.

In the table I we report for different θ, the values of the variable $\eta^2 \lambda_0/2$ for which we performed numerical simulations and fit, and the corresponding values of t_{min}, t_{max}.

Avalanche effect We have just discussed that it exists a time t_{max} over which the Shigesada-Kawasaki equations are not valid anymore. Indeed, for $t > t_{max}$ avalanche effects arise. This is due to the high emission rate and means that not only we can have multiple coalescences, (that is more colonies absorbed in a single time step), but the increase in the radius produced by these coalescences can bring to other coalescences before

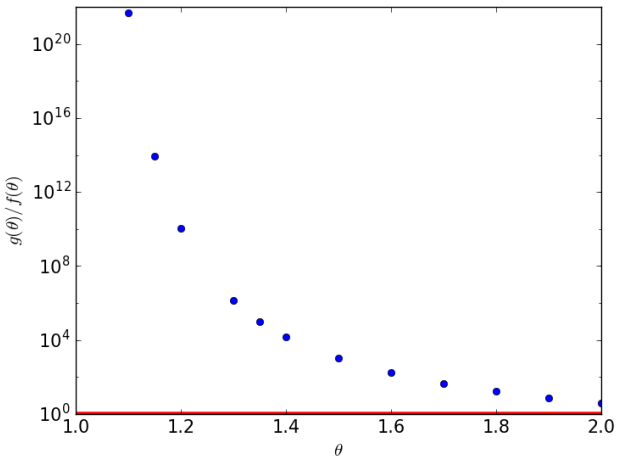


FIG. 9: $g(\theta)/f(\theta)$ **versus** θ**.**

	$\theta = 1.1$	$\theta = 1.2$	$\theta = 1.3$	$\theta = 1.4$	$\theta = 1.6$	$\theta = 2.0$
$\frac{\eta^2\lambda_0}{2}$	0.5	0.8	2.2	2.2	5	20
t_{min}	3×10^{-16}	5×10^{-7}	6×10^{-3}	5×10^{-2}	1.74	30
t_{max}	1.5×10^{6}	5.7×10^{3}	8.1×10^{3}	7.7×10^{2}	2.9×10^{2}	1.2×10^{2}

TABLE I: In the table we report for the different θ, the values of the variable $\eta^2\lambda_0/2$ for which we performed the fit, and the corresponding values of t_c, t_{max}.

moving to the next time step. Every time this happens we say that we observe an avalanche. In this situation the Shigesada-Kawasaki equations do not held and another treatment of the problem is necessary. This goes beyond the aim of this paper, however we performed numerical simulations to highlight this phenomenon, with the choice of $\theta = 1.4$. At each time step $dt = 0.001$ we count the number of avalanches n_a and the number of total coalescences n_c happened during dt as consequence of the different avalanches.
The plots are shown in Fig. 10(a-b) where we observe that at a given time around $t \approx 2000$, the avalanche phenomenon change behavior acquiring more relevance, and bringing to a change in the slope characterizing the behavior of $r(t)$ with time (see Fig. 10-c).

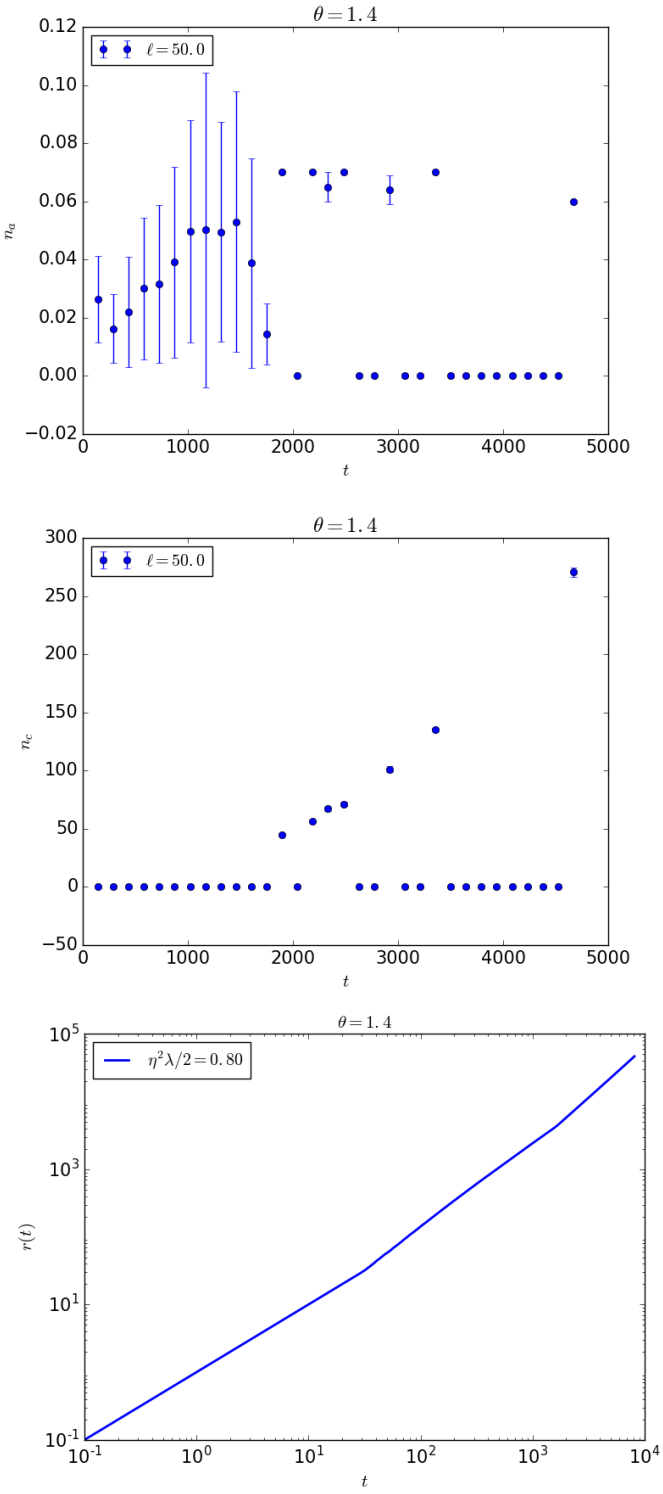


FIG. 10: (Top) n_a vs. t (Middle) n_c vs. t. (Bottom) $r(t)$ vs. t. The results are obtained averaging over 100 simulations. For $\theta = 1.4$, $\ell = 50$, $c = 1$, $\lambda = 0.001$.

The M_1 model: further empirical results

Case $\theta = 0$

We present here further simulation results obtained for the M_1 model with a constant emission rate $\lambda(r) = \lambda_0$. We assume that the area A and the perimeter P of the primary colony obey to a power-law scaling of the form

$$A(t) \sim t^{\mu} \qquad P(t) \sim t^{\nu} \ . \tag{38}$$

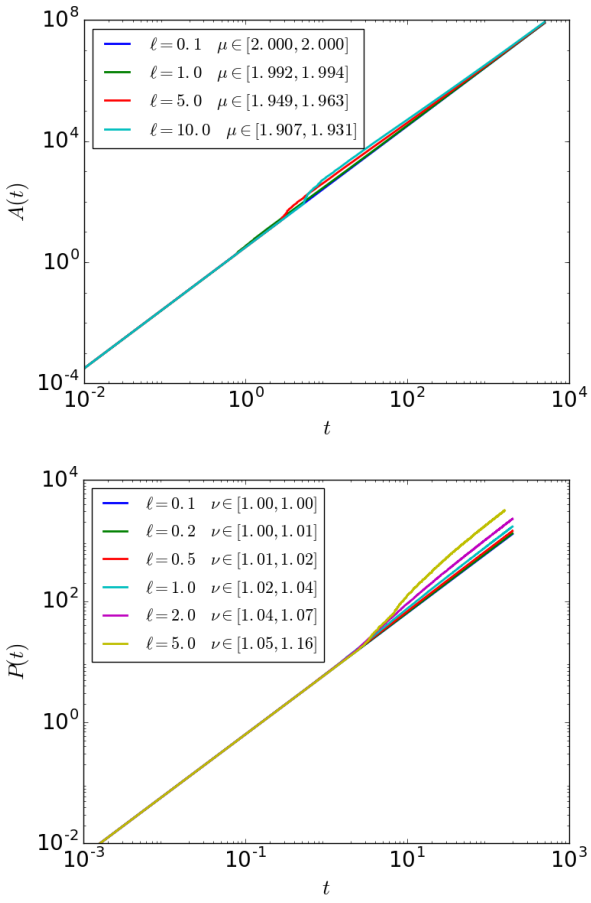


FIG. 11: (Top) $A(t)$ vs. t. (Bottom) $P(t)$ vs. t. For different values of ℓ we plot in a log-log scale, the area and the perimeter of the primary colony versus time averaged over 10 simulations. We perform a power-law fit and the values of the exponents obtained are shown in the insets.

In Fig. 11 we perform a power-law fit on the empirical results for two different time regimes. This allows us to examine eventual finite-size effects: we choose $t > t_{fc}$ and then $t > 100 t_{fc}$, with t_{fc} being the time at which the first coalescence happens. The values of the exponents μ and ν are shown in the insets of Fig. 11, with the higher value corresponding to the choice $t > 100 t_{fc}$.

We assume that the sub-dominant corrections are described by the scaling forms

$$\frac{A(t)}{\pi c^2 t^2} - 1 \sim t^{-\gamma} \qquad \frac{P(t)}{2\pi c t} - 1 \sim t^{-\gamma'} \ . \tag{39}$$

In the Table II we report for the different choice of ℓ, the values of t^* and of the exponents γ and γ'. For each value of ℓ the smaller value of the exponent correspond to the fit for $t > t^*$ and the larger value to the fit range $t > 10 t^*$.

	$\ell = 0.10$	$\ell = 1.0$	$\ell = 5.0$	$\ell = 10.0$
γ	$0.53 - 0.53$	$0.55 - 0.57$	$0.54 - 0.56$	$0.52 - 0.54$
γ'	$0.54 - 0.55$	$0.56 - 0.58$	$0.55 - 0.58$	$0.53 - 0.55$
t^*	10	30	70	100

TABLE II: In the table we report for the different choice of ℓ, the values of t^* and of the exponents γ and γ'. For each value of ℓ the smaller value of the exponent correspond to the fit for $t > t^*$ and the larger value to the fit range $t > 10 t^*$.

Case $\theta = 1$

The simulations results for the area $A(t)$ and the perimeter $P(t)$ of the primary colony, obtained for different values of ℓ are shown in Fig. 12. We assume the power-law behaviors given by Eq. (38) and we perform a fit on the empirical data. The values of the exponents obtained (for the time range $t > t_{fc}$ and $t > 20 t_{fc}$, with t_{fc} the time at which the first coalescence happens) are shown in the insets of Fig. 12. The higher values correspond to the choice $t > 20 t_{fc}$ and this suggests that, taking possible finite-size effects into account, one can write

$$\mu \approx 2 \qquad \nu \approx 1 \ . \tag{40}$$

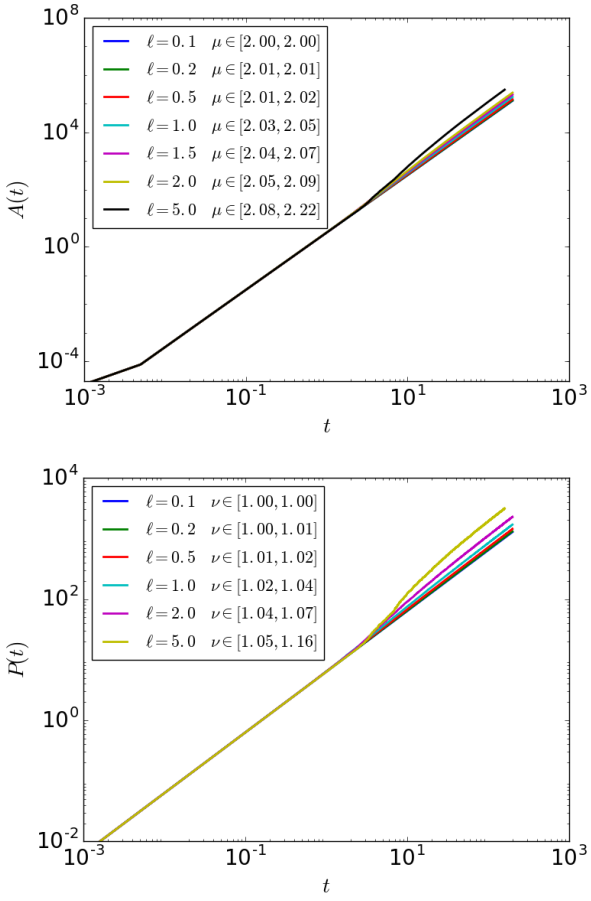


FIG. 12: (Top) $A(t)$ vs. t. (Bottom) $P(t)$ vs. t. For different values of ℓ we plot in a log-log scale, the area and the perimeter of the primary colony versus time averaged over 100 simulations. We perform a power-law fit and the values of the exponents obtained are shown in the insets.